



This is a repository copy of *Formation of white etching cracks at manganese sulfide (MnS) inclusions in bearing steel due to hammering impact loading*.

White Rose Research Online URL for this paper:  
<http://eprints.whiterose.ac.uk/98592/>

Version: Accepted Version

---

**Article:**

Bruce, T., Long, H. [orcid.org/0000-0003-1673-1193](https://orcid.org/0000-0003-1673-1193), Slatter, T. [orcid.org/0000-0002-0485-4615](https://orcid.org/0000-0002-0485-4615) et al. (1 more author) (2016) Formation of white etching cracks at manganese sulfide (MnS) inclusions in bearing steel due to hammering impact loading. *Wind Energy*, 19 (10). pp. 1903-1915. ISSN 1095-4244

<https://doi.org/10.1002/we.1958>

---

This is the peer reviewed version of the following article: Bruce, T., Long, H., Slatter, T., and Dwyer-Joyce, R. S. (2016) Formation of white etching cracks at manganese sulfide (MnS) inclusions in bearing steel due to hammering impact loading. *Wind Energy*, doi: 10.1002/we.1958., which has been published in final form at <http://dx.doi.org/10.1002/we.1958>. This article may be used for non-commercial purposes in accordance with Wiley Terms and Conditions for Self-Archiving (<http://olabout.wiley.com/WileyCDA/Section/id-820227.html>).

**Reuse**

Unless indicated otherwise, fulltext items are protected by copyright with all rights reserved. The copyright exception in section 29 of the Copyright, Designs and Patents Act 1988 allows the making of a single copy solely for the purpose of non-commercial research or private study within the limits of fair dealing. The publisher or other rights-holder may allow further reproduction and re-use of this version - refer to the White Rose Research Online record for this item. Where records identify the publisher as the copyright holder, users can verify any specific terms of use on the publisher's website.

**Takedown**

If you consider content in White Rose Research Online to be in breach of UK law, please notify us by emailing [eprints@whiterose.ac.uk](mailto:eprints@whiterose.ac.uk) including the URL of the record and the reason for the withdrawal request.



[eprints@whiterose.ac.uk](mailto:eprints@whiterose.ac.uk)  
<https://eprints.whiterose.ac.uk/>

# **Formation of white etching cracks at manganese sulphide (MnS) inclusions in bearing steel due to hammering impact loading**

**T. Bruce, H. Long\*, T. Slatter, R. S. Dwyer-Joyce**

**Department of Mechanical Engineering, The University of Sheffield, United Kingdom**

\*h.long@sheffield.ac.uk

Tel: +44 (0) 114 222 7759

Fax: +44 (0) 114 222 7890

Wind turbine gearbox bearings (WTGBs) are failing prematurely, leading to increased operational costs of wind energy. Bearing failure by white structure flaking (WSF) and axial cracking may both be caused by the propagation of white etching cracks (WECs) and have been observed to cause premature failures, however their damage mechanism is currently not well understood. Crack initiation has been found to occur at subsurface material defects in bearing steel, which may develop into WECs. One hypothesis for WEC formation at these defects, such as non-metallic inclusions, is that repetitive impact loading of a rolling element on a bearing raceway, due to torque reversals and transient loading during operation, leads to high numbers of stress concentrating load cycles at defects that exceed the material yield strength.

In this study, a number of tests were carried out using a reciprocating hammer type impact rig. Tests were designed to induce subsurface yielding at stress concentrating manganese sulphide (MnS) inclusions. The effects of increasing surface contact stress and number of impact cycles, with and without surface traction, were investigated. Damage adjacent to MnS inclusions, similar to that observed in a failed WTGB raceway was recreated on bearing steel test specimens. It has been found that increasing the subsurface equivalent stresses and the number of impact cycles both led to increased damage levels. Damage was observed at subsurface equivalent stresses of above 2.48 GPa after at least 50,000 impact cycles. WECs were recreated during tests that applied surface traction for 1,000,000 impacts.

## **Keywords**

Wind turbine gearbox, hammering impact loading, overload, bearing failure, white etching crack, white etching area, manganese sulphide (MnS) inclusion.

# 1. Introduction

During the past 15 to 20 years the wind energy industry has rapidly expanded, a trend that will continue throughout this decade. The European Wind Energy Agency (EWEA) has a planned target of 230 GW of installed wind power capacity by 2020, representing 20% of total EU electricity consumption [1]. This expansion is being limited by the high operating cost of wind energy, which is made more expensive by a number of maintenance issues, most critically concerning wind turbine gearboxes (WTGs) which are not reaching their anticipated lifespan of 20 years. It is estimated that operation and maintenance (O&M) account for 20% of the cost of offshore wind energy in the EU [2, 3].

The majority of WTG failures initiate in the wind turbine gearbox bearings (WTGBs) [4], and the exact modes of their failure are currently not well understood despite intensive research effort. This study will investigate a mode of failure that is commonly found within failed WTGBs named white etching cracking, which is described in more detail in the following section. A reciprocating hammer type impact test rig was used to initiate subsurface cracks at MnS inclusions and under certain conditions, created white etching cracks (WECs) at the inclusions. Different factors that may affect the probability of MnS inclusion initiated damage were investigated, namely: number of impact cycles, subsurface equivalent stress level and surface traction by introducing simultaneous sliding and impact loading, termed as compound impact in this study.

## 1.1. White etching cracks

Currently, the mechanism by which WECs lead to WTGB failure is not fully understood, and hence there is no method of calculating remaining useful bearing life due to the failure in WTG applications [5, 6, 7, 8]. "White etching" refers to the colour of the altered steel microstructure, after having been etched in nitric acid/ethanol solution (nital) [9]. WECs may form irregular crack networks, named "irregular white etching areas" (IrWEAs) and follow pre-austenite grain boundaries [6]. These crack networks form up to the depth of maximum shear stress, occurring over large subsurface areas and eventually leading to failure by flaking of material from the surface, also known as white structure flaking (WSF). IrWEAs have been observed to propagate radially from straight-growing cracks that are parallel to the surface in the axial direction. Through-hardened bearings are prone to fail via the axial cracking mode, whereas carburised bearings with less than 20% retained austenite fail by WSF [6]. If this WEA weakens the near-surface of the raceway sufficiently, failure occurs via spalling. White etching cracking leading to WSF is a mode of damage that can lead to bearing failure within 1-20% of the  $L_{10}$  design life [3] predicted by current bearing design standards [10].

Under high loading, stress concentration around material defects may result in yielding of the bearing steel. As a result, crack initiation may occur at the location of maximum equivalent stress around the stress concentrating material defect. Surface traction caused by the overrolling of a rolling element shifts the position of these subsurface stress concentrations around material defects. Finite element analysis software *Abaqus* was used to illustrate stress concentration around an arbitrarily sized material defect (in this case a circular void as an example). The positions of maximum equivalent stress around the void under compressive load are shown in Figure 1a. Figure 1b shows how the introduction of surface traction shifts this stress field around the void, and as a result, the positions of maximum subsurface equivalent stress in the material subsurface.

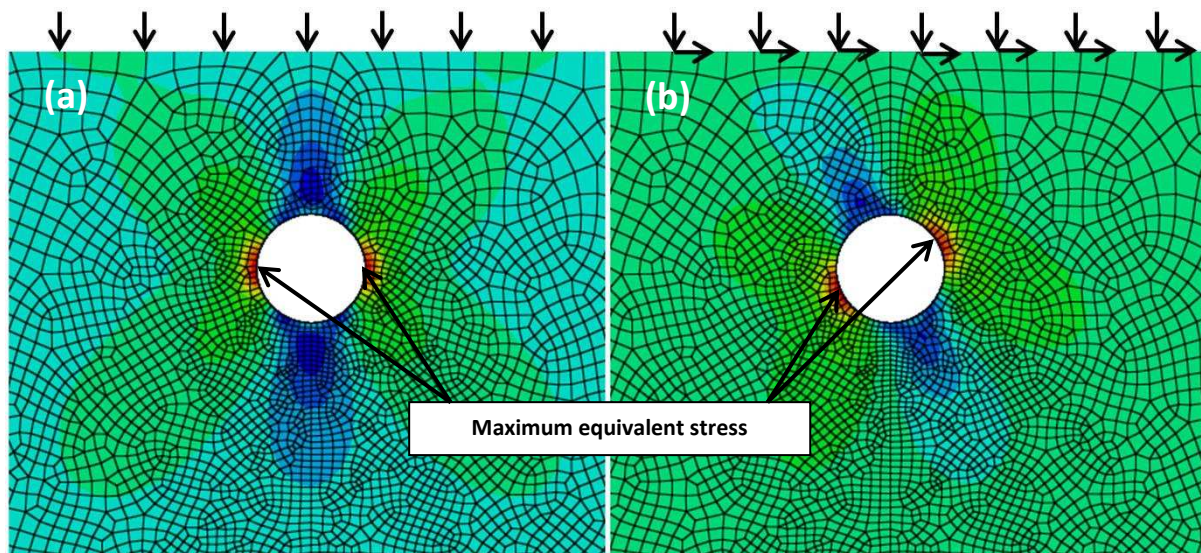


**Figure 1: Stress concentrations around a void under (a) arbitrary compressive load: (b) arbitrary compressive load and arbitrary surface traction (load directions indicated by arrows above plots)**

WEAs have been observed to form around “butterfly cracks”, named such due to their two-dimensional appearance. In this case, cracks initiate and propagate between  $30\text{-}50^\circ$  and  $130\text{-}150^\circ$  from the overrolling direction, which may be due to the position of maximum unidirectional shear stress (explained in detail in [5]). These cracks are known as “butterfly wings”. During torque reversals caused by extreme and transient loading conditions, symmetric cracks may form at the same angles, in the direction opposite to overrolling [5].

Repeated exposure to high stress levels causes dislocation accumulation at defects, forming three-dimensional crack networks around these defects, with altered microstructural properties and the appearance of “butterfly wings” [5, 6]. Evans et al. [9] conducted rolling contact fatigue tests using twin discs made from bearing steel, and that found butterfly cracks had initiated at material defects between 30 and 800  $\mu\text{m}$  below the contact surface. These “butterflies” were found to propagate into WEC networks, which themselves act as stress concentrators, due to their comparatively high hardness, 30-50% higher than the surrounding matrix [3, 11, 12]. WECs therefore propagate themselves under high loading, due to stress concentrations at the crack tip. Hydrogen embrittlement generated by lubricant aging, water contamination, or hydrogen initially present in the steel microstructure, can accelerate this process [5, 13, 14].

## **1.2. Crack initiation at manganese sulphide (MnS) inclusions in steel**

MnS inclusions have been classified into three types since 1938 [15]. Although initially the classification applied to cast steels, it has been extended to include wrought steels. Type I inclusions are globular in shape and appear in steels with practically no aluminium content. Type II are dendritic chain formations on grain boundaries and appear with the first traces of aluminium (0.005 wt%). Type III are strings of broken silicates and initially appear alongside Type II at levels of 0.01% - 0.03 wt% aluminium. At levels greater than 0.04 wt%, Type III is the only MnS inclusion to appear [15].

Typical bearing steel has very little aluminium content [16], so it is therefore globular Type I MnS inclusions that are most commonly found, although Type II and III may also be found. MnS inclusions

in hot-rolled steels are randomly distributed and of irregular shape. During manufacture, the MnS inclusions are flattened and elongated in the direction of rolling [15]. All inclusions may act as crack initiation sites under high enough contact stress [17], however in the case of white structure flaking in WTGBs, MnS inclusions have been found to be the most likely to interact with white etching crack (WEC) damage [18]. It has been found that shorter inclusions are more likely to initiate damage than longer inclusions, with the ideal length for crack propagation found to be smaller than 20  $\mu\text{m}$  (based on a sample size of 76 WEC-interacting inclusions) [18]. During quenching of bearing steel, the different thermal contraction rates of the bulk material and MnS inclusions may weaken the bond between the inclusion and the surrounding bulk material [9], or possibly lead to the creation of free surface at the inclusion/steel boundary [17]. These free surfaces are potential sites for inclusion separation from the bulk material and for initiating cracking under cyclic loading [17].

Although weakly bonded inclusions and free surfaces may be potential crack initiation sites, it is not necessary for a MnS inclusion to initiate a crack because of the poor bond with the bulk material. A thin, flattened MnS inclusion may itself act as a virtual crack [19] that may propagate into an actual crack. In rail steel, MnS inclusions can become significant crack initiators [20]. It was found that near to the rail surface, all MnS inclusions were deformed first in the material displaced direction, moved to the shear angle caused by over-rolling, and then flattened as they reached the wear surface. Wear tests on four rail steel types confirmed that almost all deformed MnS inclusions near to the wear surface were associated with cracks [19].

MnS inclusions became elongated under load because they deform more than the surrounding matrix [21, 22]. Cracks can be initiated along the highly deformed flattened MnS inclusions [21], due to: (1) micro-crack initiation at localised deformation bands in the vicinity of the inclusions; (2) high stress concentration in the middle of the elongated inclusions leading to interfacial debonding and void formation, which are potential crack initiation sites; (3) break up the inclusions because of its lower plastic limit, causing the cracks to form within the inclusion [22], which may propagate into the bulk material [18]; or (4) by high stress concentration at the lowest radius of curvature inclusion tips that coincide with the position of maximum subsurface equivalent stress as shown in Figure 1.

It has been found that one method of WEC initiation at MnS inclusions is by the propagation of cracks that are initiated within the inclusion, and spread into the surrounding material [11, 18]. WECs may then develop along the cracks [11]. It has been found by the authors, in a related study [23], that it is not necessarily the case that they must be cracked along their major axis in order to form a WEA as shown in Figure 2f, but may also form at cracks caused by other factors previously discussed. This process is illustrated in Figure 2, which shows optical microscopy and SEM images taken of MnS inclusions from a failed WTGB provided for destructive investigation [23], in which WEC initiating MnS inclusions were found at depths of up to around 600  $\mu\text{m}$  from the raceway surface. In this study, the vast majority of inclusion initiated damage, and all inclusion initiated WEC damage, was caused at MnS-type inclusions. Such damage was observed when viewing inclusions sectioned through the bearing axial and circumferential directions. Crack initiation around MnS inclusions and short crack growth can be explained by Mode I loading (normal to crack growth direction). Further growth of the cracks governed by Mode II/III shear loading (in-plane shear/off-plane shear) [9, 23, 24]. Shear loading increases in bearings under the influence of surface traction, caused by skidding of the rollers on the raceway surface [5]. It is possible that WECs require a certain level of surface traction in order to form.

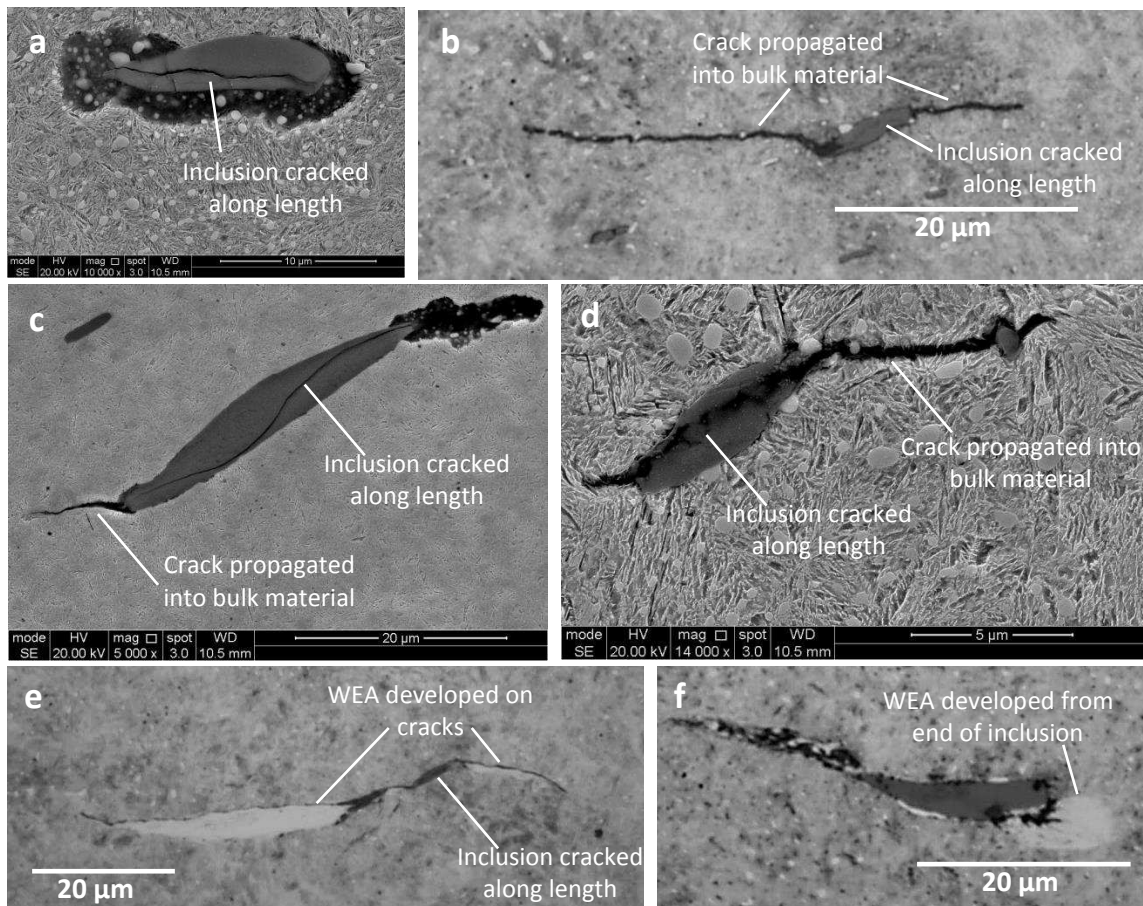


**Figure 2: Crack development at MnS inclusions from a failed WTGB a) Cracked along length of inclusion b) Crack propagated into bulk material c) & d) Split inclusion with crack propagating into bulk material e) WEA developing at split MnS inclusion e) WEA developing at MnS inclusion with no split (adapted from [23]). Images (a) and (f) are from axially sectioned specimens (over-rolling direction into the page), images (b)-(e) are from circumferentially sectioned specimens (over-rolling direction left to right).**

### 1.3. Hammering impact hypothesis

The transient nature of the wind and operational loading of a WT creates extremely harsh operating conditions for drivetrain components leading to subsurface material plastic deformation [3, 11]. The high variability of wind conditions and subsequent turbine controls leads to frequent connections and disconnections between the generator and grid, causing the gearbox to experience frequent torque reversals and overloads [25]. Such torque reversals can occur approximately 15,000 times per year [25], and in extreme cases, contact stress levels may exceed 3.1 GPa [11], well above the yield strength of bearing steels [17]. Maximum recommended contact pressures from the wind turbine design standard [26] are regularly exceeded, even during normal operating conditions [27].

A number of studies have been carried out using test rigs to recreate butterflies and/or WECs in bearing steel. Both Lund [28] and Grabulov [29] successfully recreated butterflies finding that a contact stress threshold must be exceeded for their initiation. Evans et al. [30] recreated WECs on hydrogen charged specimens under rolling contact fatigue at contact pressures between 1.2-2.0 GPa. Further work from Evans [18] created WECs in a tested WTGB under transient conditions with maximum contact pressures of 2.15 GPa.

During operation, WTGBs are more heavily loaded in the “loaded zone”, within which rollers experience high traction forces and are well aligned. In the unloaded zone, however, traction forces are much lower, resulting in poor roller alignment. An instantaneous change in shaft loading from a torque reversal relocates the loaded zone, resulting in impact loading applied to the raceway by misaligned rollers. A small misalignment angle will alter what is normally a line contact between the roller and raceway to a point contact, which will lead to far higher contact stresses on a small area of the raceway. Based on the influencing factors reported in the literature, the following damage mechanisms leading to WEC formation by the hammering impact loading hypothesis are proposed by the authors, as listed in Table 1. Those mechanisms and factors highlighted in bold are investigated in this study.

Root Cause	Proposed Damage Mechanisms	Factors Reported in the Literature
High contact stress/hammering impact loading	<ul style="list-style-type: none"> <li>- <b>Hammering impact loading from torque reversals leads to high contact stresses</b></li> <li>- <b>Crack initiation due to stress concentration at inclusions</b></li> <li>- <b>Separation of inclusions from steel matrix</b></li> <li>- <b>Crack initiation at inclusions (Mode I loading)</b></li> <li>- <b>WEC propagation from inclusions (Mode II/III loading)</b></li> <li>- <b>Eventual failure by axial cracking of raceway or WSF</b></li> </ul>	<ul style="list-style-type: none"> <li>- <b>Contact stress level (impact energy)</b></li> <li>- <b>Number of impacts (load cycle)</b></li> <li>- Misalignment</li> <li>- Bearing location</li> <li>- Lubricant decomposition</li> <li>- % retained austenite</li> <li>- Hydrogen embrittlement</li> <li>- Residual stress</li> <li>- <b>Inclusions/voids/carbides</b></li> <li>- Carburised/Through-hardened</li> <li>- <b>Skidding (surface traction)</b></li> </ul>

**Table 1: Summary of damage mechanisms and factors affecting the development of WECs at inclusions in WTGBs**

## 2. Hammering impact testing

Hammering impact testing was designed in order to investigate the effect of repeatedly exposing bearing steel to high contact stresses in a controlled environment. Testing to investigate the following key factors was undertaken:

1. If repetitive impacts alone cause WEA and butterfly crack formation in bearing steel (normal impact).
2. If the extent of damage is affected by varying the number of impacts (loading cycles).
3. If the extent of damage is affected by varying the contact stress (loading levels).
4. If sliding at contacting surfaces during impact has an effect on the extent of damage caused (compound impact).

A test rig that was developed by Slatter and used extensively for previous work of material surface wear [31, 32, 33] was modified for use in this study as shown in Figure 3a. The rig provided a repeatable way to apply a set level of impact force to a specimen, at a set impact angle, at set time intervals for a set number of impact cycles. Compound impact was introduced by using a separate striker component, which was angled at 45° allowing the impacting ball to slip along the specimen surface during impact. The specimen and striker were aligned so that the impacting ball hit its surface at an angle of 45° as shown in Figure 3b. The main modifications to the rig were:

1. The development of a new specimen holder that operates like a vice, to clamp cylindrical test specimens (45 mm diameter, by 10 mm width) in position under the striker component as

shown in Figure 3. Note that the position of the specimen is such that the impacting ball hits the specimen normal to its surface.

2. The attachment of the “mass holder” plate onto the “pivot block”, allowing for counterweights to be attached to the arm, altering the effective mass of the “striker” in order to vary the impact load levels.

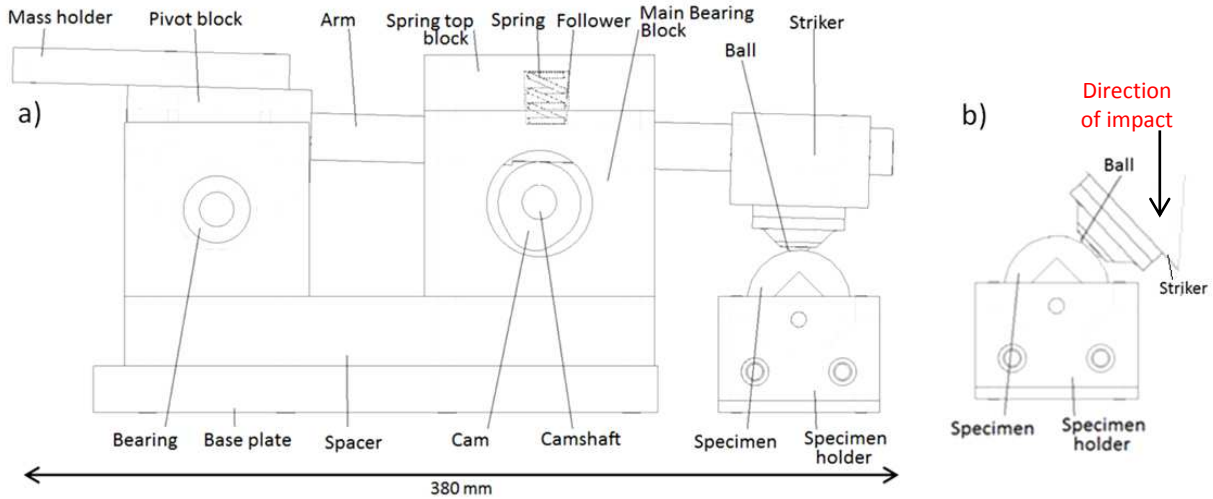


Figure 3: Modified impact test rig a) normal impact b) compound impact

## 2.1. Tested specimens

Through-hardened 100CrMo7 bearing steel specimens were tested using the hammering impact rig. Before testing, the specimens were quenched then tempered at 260 °C, to achieve a hardness of around 60 HRC. The surface was ground to give a maximum roughness,  $R_a$ , of 1 micron. The material was selected for its yield strength and hardness properties, which were suited to the capabilities of the test rig so that subsurface damage could be caused, without significant surface damage. The steel balls used to impact the specimens were slightly harder than the specimens, so that damage was first experienced on the specimens. The approximate chemical composition of non-FE elements found in the specimens is shown in Table 2 [34] and the mechanical properties of both the specimens [17] and the impact steel ball, in Table 3.

C%	Si%	Mn%	S%	Cr%	Ni %	Mo%
0.99	0.30	0.70	0.015	1.80	0.13	0.25

Table 2: Chemical composition of specimens used during testing

	100CrMo7 (specimen)	100Cr6 (impact ball)
Young's modulus	210 GPa	210 GPa
Hardness	59-61 HRC	60-67 HRC[33]
Yield strength	1.7 GPa	~2 GPa
Tensile strength	2.4 GPa	~2.3GPa
Poisson's ratio	0.3	0.3
Density	7800 kg/m <sup>3</sup>	~7800 kg/m <sup>3</sup>
Diameter	45 mm	15 mm
Surface roughness, $R_a$ (max)	1 $\mu$ m	0.125 $\mu$ m [33]

Table 3: Mechanical properties of specimens [17] and impact steel balls used during testing (Approximate 100Cr6 properties from [17])

As previously discussed, it is important to consider the orientation of MnS inclusions in bearing raceways. Inclusions in the specimens were orientated with their longest dimension orientated parallel to the axis of the test specimens, as shown in Figure 4. The chemical composition of a number of MnS inclusions from the specimens was tested to verify their composition. Element weight and atomic percentages of a typical inclusion are shown in Figure 5. After testing the specimens were sectioned in the axial direction, mounted in conductive bakelite resin, ground to the level of the centre of the impact zone, polished to a surface roughness of 0.06  $\mu\text{m}$  and etched in 2% nital solution, before observation took place using both optical and scanning electron microscopy. All inclusions within the section made through the impact zone were observed and photographs were taken of those that had initiated damage. All measurements of inclusion lengths and their depths from the contact surface were made using the measurement tool built into the control software of the microscopes used. Six examples of MnS inclusions in an undamaged specimen are displayed in Figure 6 for comparison to damaged inclusions discussed in section 3. The inclusions in the undamaged specimen display no damage from the heat treatment or sectioning processes. Although other inclusion types were found within the specimens, only MnS-type inclusions were found to have initiated damage.

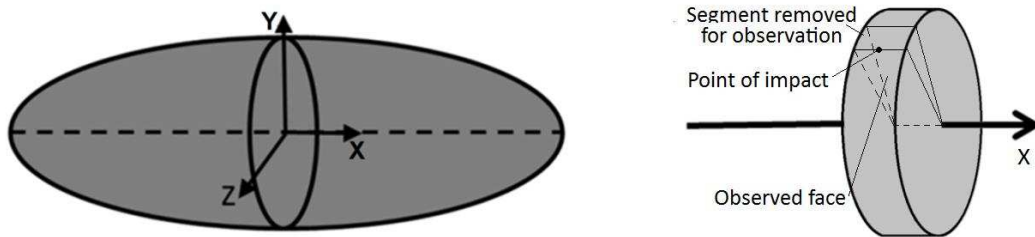


Figure 4: Orientation of MnS inclusions in specimens

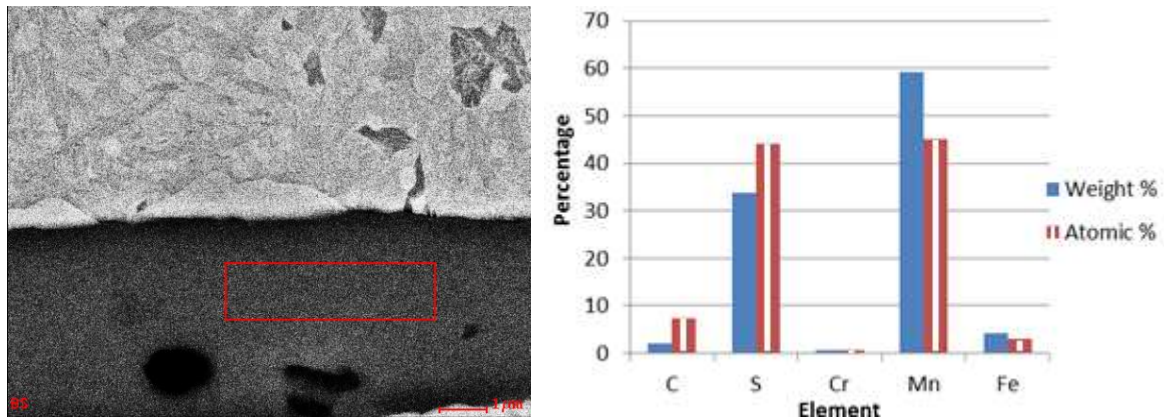


Figure 5: Weight and atomic percentages of an example MnS inclusion from a hammering impact specimen

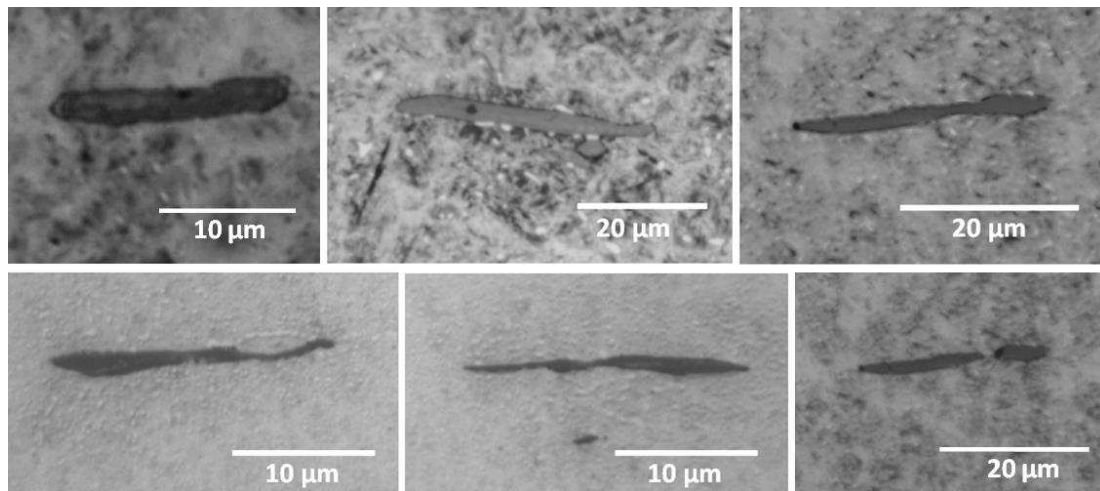


Figure 6: Typical MnS inclusions in undamaged specimen

## 2.2. Test design using finite element analysis

As shown in Figure 2, one form of WEC damage can initiate at defects below the raceway surface. Therefore, it seems logical to design experiments that create subsurface plastic deformation, but do not exceed the material yield strength on the surface. Commercial software Abaqus was used in Finite Element Analysis (FEA) to simulate the impact between the steel ball and specimen. Explicit analysis was used to model the contact stresses caused by the impact of a correctly dimensioned steel ball, with the effective mass of the striker, upon a specimen. **The steel ball was given velocity equal to the velocity of impact for each test condition and the resulting contact pressures during impact were calculated by the dynamic FEA model.** The material properties listed in Table 3 along with its stress-strain behaviour, were used to define the material. The stress-strain curve found from a tensile test of through hardened 100Cr6 bearing steel (also tempered at 260 °C) was used [35], which has very similar stress-strain behaviour to 100CrMo7 bearing steel [34]. Compressive stress-strain data was not available and although tensile behaviour cannot accurately model compressive behaviour close to the material's ultimate strength, it has been assumed that the results are accurate enough to approximate the surface contact stress, which is below the yield strength of the material for all tests and is the key result from FEA simulations. Maximum stress levels on the surface and subsurface were recorded from the equivalent stress (von Mises) distribution calculated using FEA.

**Contact was modelled using "hard" contact with default constraint enforcement; normal behaviour and tangential behaviour was assumed to frictionless. Surfaces were assumed to be smooth. Since contact between the two bodies is symmetrical around the centre of contact when sectioned axially (along the specimen axis) and circumferentially (through the circumference of the specimen), modelling a quarter of the lower half of the impacting ball and upper half of the specimen provided a computationally efficient way of obtaining results. Consequently, the effective mass of the ball was divided by four, since only a quarter of the contact area was available to absorb the impact energy. Since the model was designed to simulate symmetric contact about the centre of impact, it could not be used to accurately simulate sliding contact, which effectively has a moving point of impact. For this reason the simple assumption was made that the contact pressures were equal to that of a normal impact with an impact velocity equal to the radial velocity component of the sliding impact,**

defined using equation 4.3. From this, the contact pressure could be found using the normal impact FEA model.

$$U_{\text{radial}} = \frac{U_{\text{sliding}}}{\sqrt{2}} \quad (1)$$

Figure 7a shows the initial stress distribution under impact loading at the first point of contact. The stress distribution, perhaps intuitively, experiences its maximum level directly under the point of contact between ball and specimen. However, it can be seen that the equivalent stress level at the point in time when maximum contact stress is experienced, is not directly underneath the point of impact, rather, at two symmetric points either side of the centre of impact (Figure 7b). For the example shown (0.34 joules impact energy), this distance is approximately 1 mm either side of the point of impact. The implications of this are that the area around the point of impact is of interest and any features found in the microstructure away from its direct vicinity may also be linked to the hammering impact loading. The semi-circular area with a 1 mm radius around the point of impact both on the surface and subsurface, will be named the “impact zone” (IZ), and will be observed in detail for all test specimens. Table 4 shows the calculated maximum surface contact stresses and subsurface equivalent stresses for all investigated impact conditions.

Although surface roughness will have a very localised effect on the stress field, it is assumed that as it is relatively low (of the order of 1 micron), it will have very little effect on the stress distribution around relatively large MnS inclusions (of the order of 10 µm) that are some distance away from the surface (of the order of 100 µm). As a result, it seems fair to assume that the effects of surface roughness are negligible when investigating cracking at subsurface inclusions.

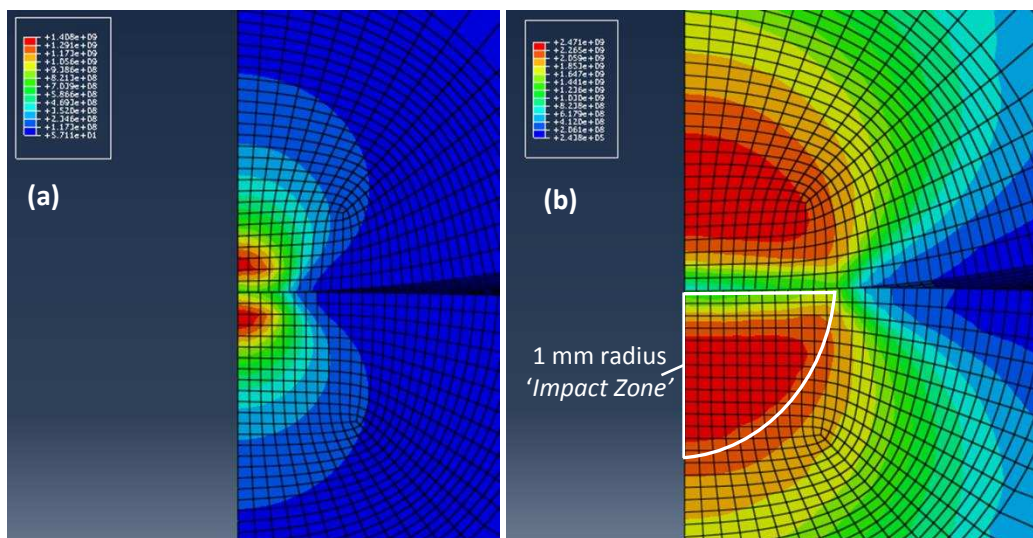


Figure 7: Equivalent stress distribution for 0.4 m/s impact velocity at (a) initial contact (b) max loading, stress unit N/m<sup>2</sup>

### 3. Test results and discussion

Hammering impact tests described by Table 4 were designed in order to investigate the above stated factors. After testing, surface inspection of the IZ revealed that there was almost no visible surface damage on any of the specimens, although a small “smoothed” mark was left where the surface oxide layer had been removed. This mark was useful to determine the exact point of impact, which was carefully marked before sectioning. It is unclear whether this small mark was caused by very low levels of plastic deformation of the surface or the removal of an oxide layer. However, as bearing contact stress in wind turbines sometimes exceeds bearing steel yield strength by significantly higher percentages than those experienced during these tests, surface plastic deformation may also occur in WTGBs. As damage was found as deep as 300  $\mu\text{m}$  below the contact surface, it is assumed that damage at inclusions is not affected by this small mark.

	Specimen number	Impact frequency (Hz)	Impact velocity (m/s)	Surface stress max (GPa)	Subsurface stress max (GPa)	Striker angle (degrees)	Test time (mins)	Number of cycles
Initial testing	1	10	0.45	1.675	2.580	90	166.7	100,000
	2	10	0.45	1.675	2.580	90	166.7	100,000
	3	10	0.45	1.675	2.580	90	166.7	100,000
TEST 1: Varying number of impacts	4	11	0.50	1.687	2.603	90	303.0	200,000
	5	11	0.50	1.687	2.603	90	227.3	150,000
	6	11	0.50	1.687	2.603	90	151.5	100,000
	7	11	0.50	1.687	2.603	90	75.8	50,000
	8	11	0.50	1.687	2.603	90	37.9	25,000
	9	11	0.50	1.687	2.603	90	18.9	12,500
TEST 2: Varying contact stress	10	3	0.14	1.540	2.153	90	277.8	50,000
	11	5	0.23	1.584	2.360	90	166.7	50,000
	12	7	0.32	1.651	2.477	90	199.0	50,000
	13	9	0.41	1.667	2.560	90	92.6	50,000
	14	11	0.50	1.687	2.603	90	75.8	50,000
TEST 3: Long term tests	15-16	11	0.50	1.687	2.603	90	1515.2	1,000,000
	17-18	11	0.35*	1.659	2.510	45	1515.2	1,000,000
	19-20	11	0.35*	1.659	2.510	45	1515.2	1,000,000

Table 4: Schedule for hammering impact testing (\*for compound impact tests, the normal component of the impact velocities are displayed for comparison).

Initial tests were carried out on specimens 1-3, which were each impacted 100,000 times, under a maximum subsurface equivalent stress of 2.58 GPa. The purpose of these initial tests was to investigate the extent of damage experienced under such conditions. Figure 8 presents examples of the damage observed at two MnS inclusions found during initial testing. This finding proved that damage was being caused under these conditions and further testing was designed in order to attempt to find the threshold at which damage begins.

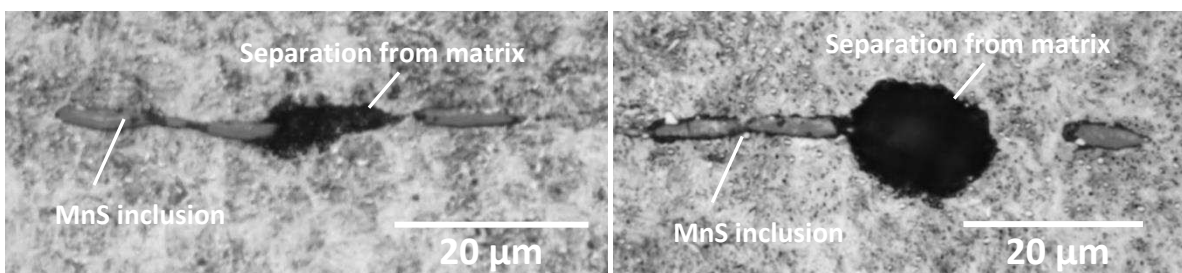
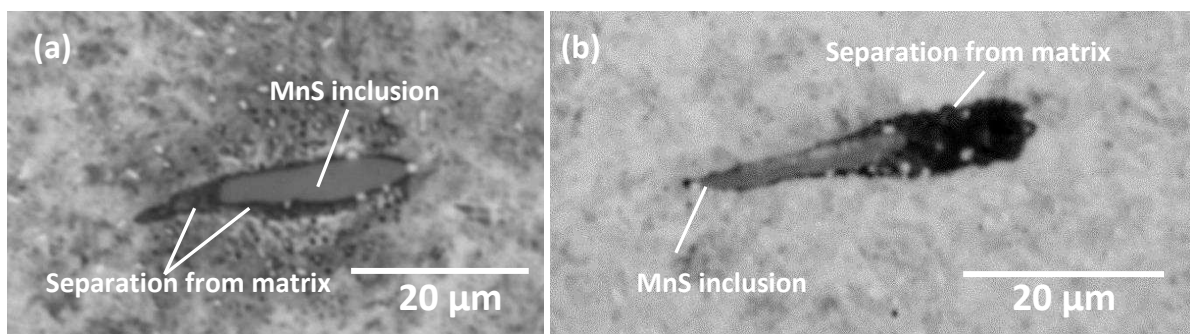


Figure 8: Examples of damage initiation at MnS inclusions during initial tests

### 3.1. Test 1: Varying number of impacts

Specimens 4-9 were impacted at the maximum equivalent stress level (2.6 GPa); the maximum that the rig could inflict under the setup described in section 2. The number of impacts was increased from 12,500 to 200,000 with higher impact numbers applied each time, test details are given in Table 4. The purpose was to observe whether the number of impacts had an effect on the quantity and the level of damage found at inclusions within the specimens.

It was clear that damage at MnS inclusions was sensitive to the number of impacts experienced. Many inclusions were found to have separated from the surrounding matrix, two examples are shown in Figure 9. Separation damage, leading to the creation of free surfaces was considerably more common in the specimens that had been exposed to more impacts. The number of damaged inclusions observed in the IZ for each specimen is shown in Figure 9.11. At least 4 inclusions had initiated damage for samples that had been exposed to over 50,000 impacts. One damage initiating inclusion was found in the specimen that had been impacted 25,000 times and none were found on the sample with 12,500 impacts. These results suggest that separation of inclusions from the matrix is very much dependent on the number of impacts experienced and that there is a threshold at which MnS inclusions separating from the surrounding material and/or to initiate cracks. After around 50,000 impacts, it seems that the material defects that may initiate damage, are likely to have done so.



**Figure 9: Examples of damage at MnS inclusions during tests at varying number of impact (a) 50,000 (b) 100,000**

### 3.2. Test 2: Varying contact stress

Specimens 10-14 were impacted 50,000 times, a quantity that was determined to be above the threshold required for subsurface damage to initiate by observing the damaged samples from Test 1. The maximum subsurface equivalent stress was increased from 2.15 GPa to 2.60 GPa (test conditions are presented in Table 4), by altering impact velocity to increase impact energy and therefore the surface contact stress level, to investigate the effect of changing this factor on the resulting damage. Two examples of damaged inclusions found during varying contact stress tests are presented in Figure 10. Figure 11 shows that as the subsurface equivalent stress increased, so did the number of damaged inclusions. There seems to be a threshold for damage initiation (not exclusively) above subsurface equivalent stresses of 2.48 GPa.

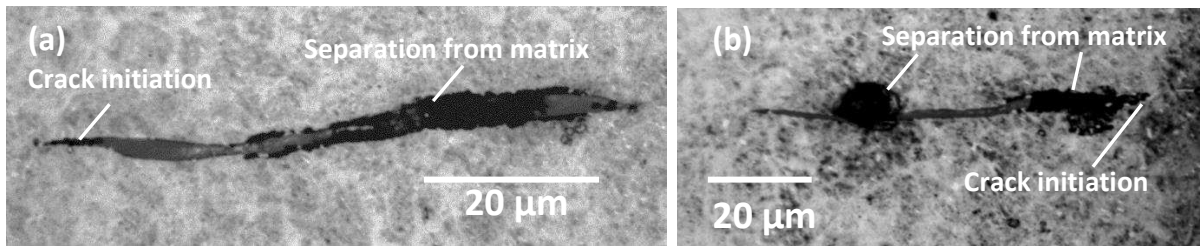


Figure 10: Example of damage at MnS inclusions during tests at varying subsurface stress (a) 2.48 GPa (b) 2.60 GPa.

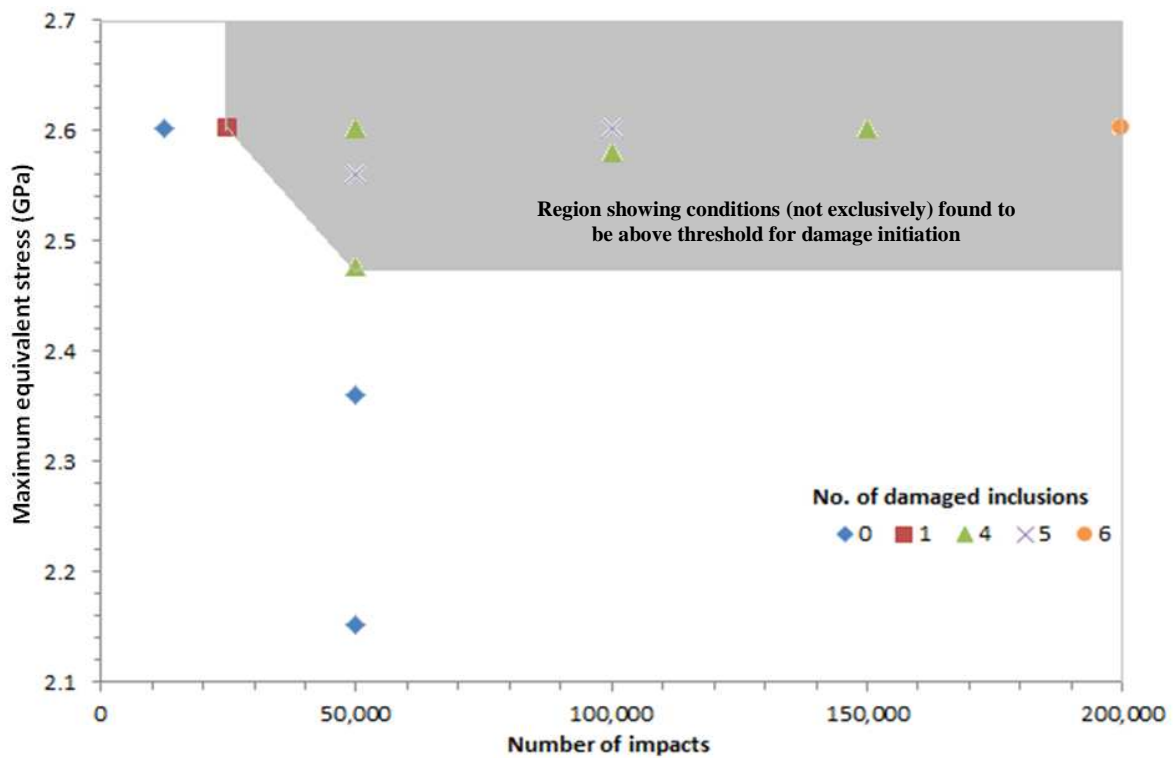
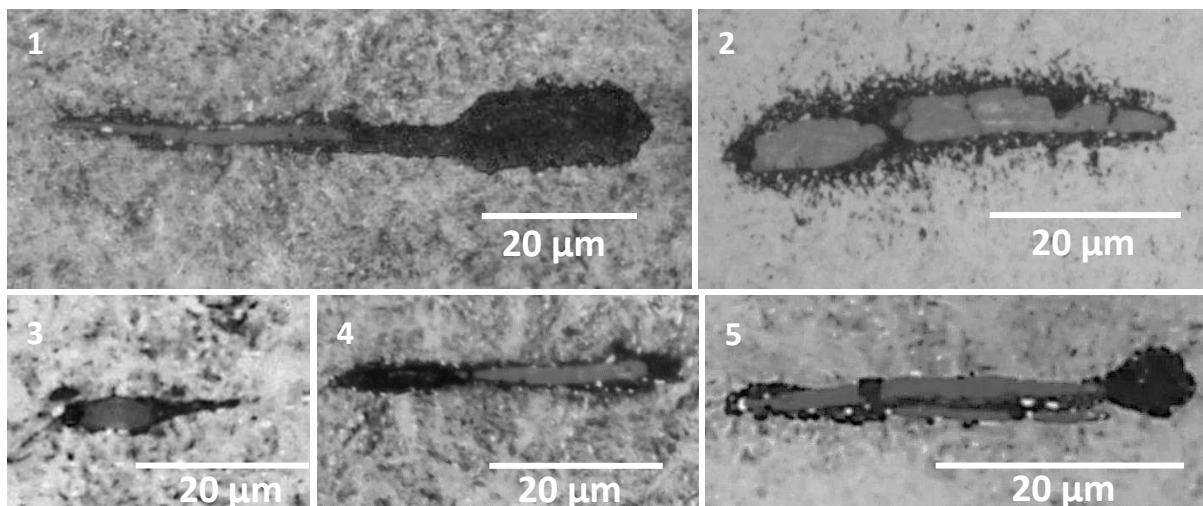


Figure 11: Number of damaged inclusions for each test when subjected to various testing conditions

### 3.3. Test 3: High cycle number tests

Six specimens were subjected to high cycle number impact tests. Each was hit 1 million times at the maximum impact energy that the test rig could provide. Two specimens were exposed to normal impact loading and four at an angle of 45 degrees (compound impact) in order to introduce surface traction. Impact angle was altered by replacing the striker shown in Figure 3 with an angled alternative. Table 4 summarises the described test schedule.

Figure 12 displays images of five damaged inclusions found at depths of up to 285  $\mu\text{m}$  beneath the surface in specimens 15 and 16 (high cycle number tests with no surface traction). Major separation, cracking of inclusions and crack initiation at inclusion tips has been observed. The table presented in Figure 12 describes the damage in more detail. In summary, although the damage in specimens 1-2 is fairly extensive, the location of the damage is fairly local to the inclusions and crack propagation has not occurred to any great extent. This is in agreement with the theory that mode 1 loading may cause crack initiation and short growth, but some shear loading is required for further propagation.

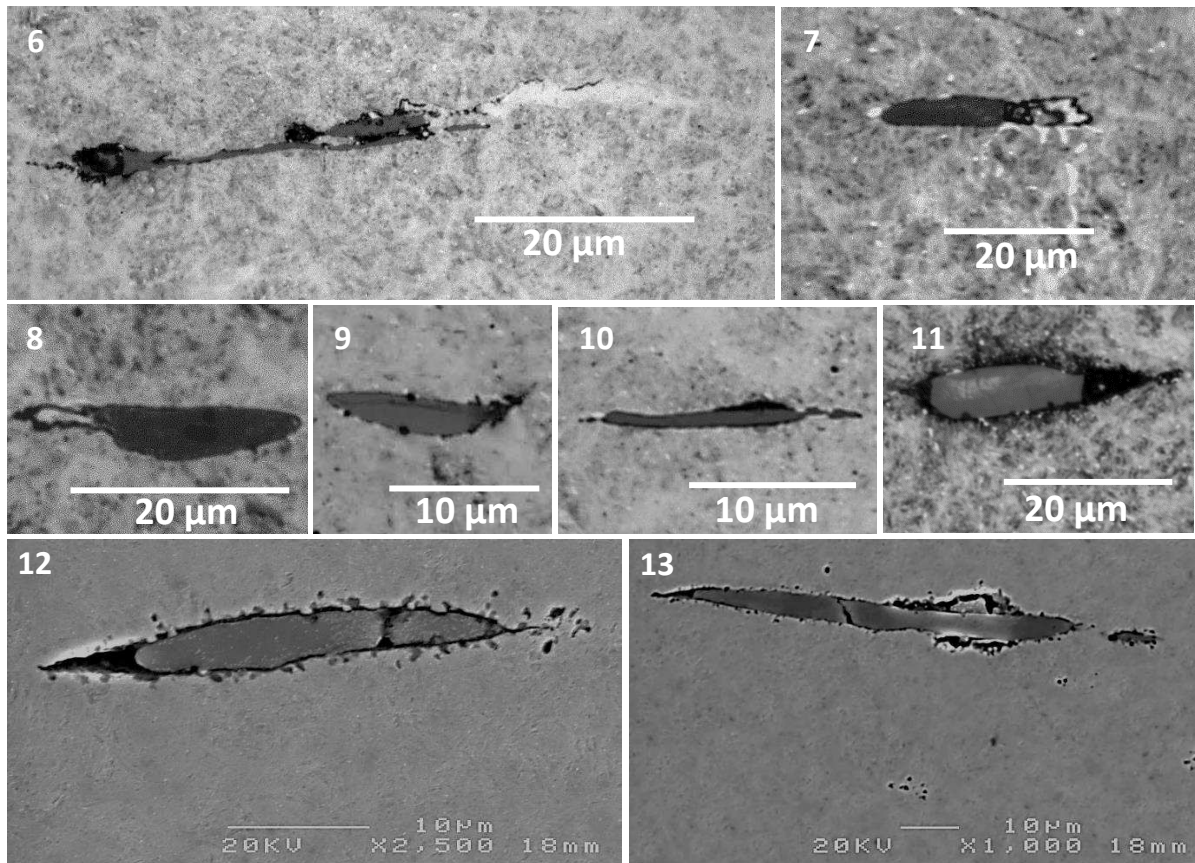


Inclusion no.	Inclusion depth ( $\mu\text{m}$ )	Inclusion length	Damage description
1	89	31	Inclusion elongated, major separation to right side
2	130	37	Major break and cracking within inclusion, separation from surrounding matrix
3	144	8	Separation on left and right, crack propagation on right side
4	285	20	Separation and possible crack propagation on left side
5	95	32	Inclusion cracked, separation to left and right, significantly to right side

**Figure 12: Five example inclusions damaged under normal impact loading of high impact cycles**

Figure 13 displays that significantly more damage was caused by compound impact testing. Damage found in specimens 15-16 was seen to a greater extent in specimens 17-20 after all specimens were impacted 1,000,000 times. A WEC was found to be connected to inclusion 6 and possibly on a number of others. Inclusion 6 was situated directly below the impact site at a depth of 98  $\mu\text{m}$ . It appears to have been internally cracked and broken up as well as initiating cracking in the bulk material from its tips and WEA formation from its right hand end. The WEA seems to have formed beneath a crack that has propagated from the right hand side. It is hypothesised that the increased levels of Mode II/III shear loading caused by the surface traction force were necessary to propagate the crack. The free surfaces created by the crack may then have rubbed against one another over thousands of shear loading cycles and caused the formation of the WEA.

Cracking was found on a number of inclusions, examples can be seen on inclusion 6, 9, 12 and 13. Inclusion 9 is cracked along its length, similarly to inclusions a-e presented in Figure 2. These findings show that compound impact creates more damage at inclusions and it may be that it is necessary in order for damage to propagate significantly into the surrounding steel matrix.



Inclusion no.	Inclusion depth (μm)	Inclusion length	Comments
6	98	38	Major break up of inclusion, separation, cracking to left and right, major WEA to right
7	93	19	Cracking and possible small WEA to right
8	290	17	Cracking and possible small WEA to left
9	111	12	Inclusion split along length, crack from right side
10	220	18	Small crack to left, separation along right side and bottom
11	106	18	Separation to left and right, crack initiation to right
12	176	24	Inclusion split vertically, separation to left, crack initiation to left and right
13	178	67	Inclusion split, separation above and below, crack initiation to left

**Figure 13: Example inclusions damaged (specimens 17-20) under compound impact testing of high impact cycles**

Comparing the sizes of damaged inclusions over the high cycle number tests shows no strong trend of damage with inclusion size. It appears that cracking can occur on inclusions of differing lengths (from 8 to 67 μm). It is the case that damaged inclusions of shorter lengths (around 20 μm) were more common than damaged longer inclusions (between 30 to 70 μm), however this is likely to be that shorter inclusions are more populous than longer inclusions in general. It is likely that proximity of inclusions to the point of subsurface maximum equivalent stress is a more important factor than inclusion length itself. **Multilife™ is a possible method to increase the lifetime of planetary WTGBs that has been developed by Ricardo PLC, whereby the nominally stationary inner raceway is periodically indexed around the planetary pin it is fitted to, thereby moving the loaded zone an distributing the wear around the entire circumference of the raceway [36].**

## 4. Conclusions

Having investigated factors affecting damage initiation caused in bearing steel under hammering impact loading and recreated white etching cracking at MnS inclusions, the following conclusions may be drawn.

1. Damage was created at subsurface MnS inclusions in bearing steel by using a reciprocating hammering impact test rig at depths of up to 290  $\mu\text{m}$  from the impact surface. Damaged inclusions were between 8 – 67  $\mu\text{m}$  in length, but were most commonly around 20  $\mu\text{m}$  long. Damage in the form of cracking of the bulk material and/or separation of the inclusion from the bulk material appears to preferentially occur at the point of lowest radius of curvature at the ends of the inclusion.
2. Increasing the number of loading cycles increased the level of damage caused, with increasing cycle numbers causing damage at a higher number of inclusions. Tests of over 50,000 impact cycles created damage at four or more inclusions in each tested sample and seemed to be a threshold for damage initiation.
3. The level of subsurface equivalent stresses correlated with the amount of damage caused, with higher stress levels causing damage at a higher number of inclusions. Tests of above 2.48 GPa consistently created damage at more inclusions and seemed to be a threshold for damage initiation.
4. Commonly observed damage features in wind turbine gearbox bearings including: the cracking of MnS inclusions along their length, the propagation of the cracks from MnS inclusions into the bulk material, the separation of MnS inclusions from the steel matrix, and the initiation and propagation of WECs. These features can be replicated by exposing bearing steel to many cycles (of the order of 1 million) of simultaneous hammering impact and surface sliding (compound impact) at subsurface equivalent stresses of approximately 2.5 GPa. It is hypothesised that surface traction is necessary for the formation of WECs due to increased cycles of Mode II/III shear loading.

## Acknowledgements

The authors would like to thank EPSRC Doctoral Training Grant (EP/J 503149/1) and Ricardo UK Limited for funding this research.

## References

1. European Wind Energy Association (2010), The European Wind Initiative: Wind Power Research and Development to 2020, Brussels
2. Arántegui, R. L., Corsatea, T. and Suomalainen, K., (2012) 2012 JRC Wind Status Report, European Commission.
3. Greco, A., Sheng, S., Keller, J., Eridemir, A. (2013) Material wear and fatigue in wind turbine systems, *Wear*, 302(1-2), 1583–1591.
4. Musial, W., Butterfield, S. and McNiff, B. (2007) Improving wind turbine gearbox reliability, National Renewable Energy Laboratory, Golden, Colorado.
5. Evans, M. -H. (2012) White structure flaking (WSF) in wind turbine gearbox bearings: effects of 'butterflies' and white etching cracks (WEC), *Materials Science and Technology*, 28(1), 3-22.
6. Errichello, R., Budny, R. and Eckert, R. (2013) Investigations of bearing failures associated with white etching areas (WEAs) in wind turbine gearboxes, *Tribology Transactions*, 56(6), 1069-1076.
7. Luyckx, J. (2011) WEC failure mode on roller bearings. Presentation at Wind Turbine Tribology Seminar, Hansen Transmissions.
8. Kotzalas, M. N. and Doll, G. L. (2010) Tribological advancements for reliable wind turbine performance, *Philosophical Transactions of the Royal Society A*, 368(1929), 4829-4850.
9. Evans, M. -H., Richardson, A., Wang, L., and Wood, R. (2013) Serial sectioning investigation of butterfly and white etching crack (WEC) formation in wind turbine gearbox bearings, *Wear*, 302 (1-2), 1573-1582.
10. International Organization for Standardization (2007), "BS ISO 281: Dynamic load ratings and rating life."
11. Gegner, J. (2011), "Tribological aspects of rolling bearing failures," in *Tribology - Lubricants and Lubrication*, INTECH, 33-94.
12. Grabulov, A., Ziese, U. and Zandbergen, H. W. (2007) TEM/SEM investigation of microstructural changes within the white etching area under rolling contact fatigue and 3-D crack reconstruction by focused ion beam, *Scripta Materialia*, 57(7), 635–638.
13. Uyama, U., Yamada, H., Hidaka H. and Mitamura, N. (2011) The effects of hydrogen on microstructural change and surface originated flaking in rolling contact fatigue, *Tribology Online*, 6(2), 123-132.
14. Vegter, R. H. and Slycke, J. T. (2010) The Role of Hydrogen on Rolling Contact Fatigue Response of Rolling Element Bearings, *Journal of ASTM International*, 7(2), 1–12.
15. Sims, C. and Dahle, F. (1938) Effect of Aluminium on the Properties of Medium Carbon Cast Steel, *AFS Transactions*, 46, 65-132.

16. British Standards Institution (2005) "PD 970:2005 Wrought steels for mechanical and allied engineering purposes. Requirements for carbon, carbon manganese and alloy hot worked or cold finished steels."
17. Bhadeshia, H. (2012) Steels for Bearings, *Progress in Materials Science*, 57, 268–435.
18. Evans, M.-H, Richardson, A., Wang, L., Wood, R. J. K. (2013) Serial sectioning investigation of butterfly and white etching crack (WEC) formation in wind turbine gearbox bearings, *Wear*, 302(1-2) 1573-1582.
19. Perez-Unzueta, A. J. and Beynon, J. H. (1993) Microstructure and wear resistance of pearlitic rail steels, *Wear*, 162-164 Part A, 173-182.
20. Dhua, S. K., Amitava R., Sen, S. K., Prasad, M. S., Mishra, K. B. and Jha, S. (2000) Influence of nonmetallic inclusion characteristics on the mechanical properties of rail steel, *Journal of Materials Engineering and Performance*, 9(6), 700-709.
21. Liu, C., Bassim, M. and Lawrence, S. (1993) Evaluation of fatigue-crack initiation at inclusions in fully pearlitic steels, *Materials Science and Engineering*, 167(1-2), 108-113.
22. Chard, A. (2011) *Deformation of inclusions in rail steel due to rolling contact*, University of Birmingham, Doctoral Thesis.
23. Bruce, T., Rounding, E., Long, H. and Dwyer-Joyce, R. S. (2015) Characterisation of white etching crack damage in wind turbine gearbox bearings, *Wear*. In press, doi:10.1016/j.wear.2015.06.008
24. Lewis, M. W. J. and Tomkins, B. (2012) A fracture mechanics interpretation of rolling bearing fatigue, *Proc. IMechE Part J: J Engineering Tribology*, 226(5), 389-405.
25. Stadler, K. and Stubenrauch, A. (2013) *Premature bearing failures in industrial gearboxes.*, SKF, Technical Report ATK 2013, Schweinfurt, Germany.
26. International Organisation for Standardization (2012) IEC 61400-4:2012: Wind turbines - Part 4: Design requirements for wind turbine gearboxes.
27. Bruce, T., Long, H., Dwyer-Joyce, R. S. (2015) Dynamic modelling of wind turbine gearbox bearing loading during transient events, *IET Renewable Power Generation*, doi: 10.1049/iet-rpg.2014.0194.
28. Lund, T. B. (2010) Sub-surface initiated rolling contact fatigue—influence of non-metallic inclusions, processing history, and operating conditions, *Journal of ASTM International*, 7(5), 1-12.
29. Grabulov, A., Ziese, U., Zandbergen, H. W. (2007) TEM/SEM investigation of microstructural changes within the white etching area under rolling contact fatigue and 3-D crack reconstruction by focused ion beam, *Scripta Materialia*, 57(7), 635–638.

30. Evans, M. H., Richardson, A., Wang, L. and Wood, R. (2013) Effect of hydrogen on butterfly and white etching crack (WEC) formation under rolling contact fatigue (RCF) *Wear*, 306(1-2), 226–241.
31. Slatter, T., Lewis, R., Jones, A. (2011) The influence of cryogenic processing on the impact wear resistance of low carbon steel and lamellar graphite cast iron. *Wear*, 271(9-10), 1481-1489.
32. Slatter, T., Lewis, R. (2010) The influence of induction hardening on the impact wear resistance of compacted graphite cast iron (CGI), *Wear*, 270(3-4), 302-311.
33. Slatter, T. (2010) *Reducing Automotive Valve Train Recession with Surface Treatment*, University of Sheffield, Doctoral Thesis.
34. Ovako (2011) Ovako 825 product specification, Issue 4
35. Fujita, S. And Murakami, Y. (2013) A New Nonmetallic Inclusion Rating Method by Positive Use of Hydrogen Embrittlement Phenomenon, *Metallurgical and Materials Transactions A*, 44(1) 303-322.
36. Wheals, J. C., Guern, P., Dwyer-Joyce, R. S., Marshall, M. and Howard, T. (2011) Ricardo MultiLife™ Bearing Programme for Increased Reliability of Offshore Wind Turbines, *European Wind Energy Conference 2011*, Brussels.